Numerical Homogenization of Bone Microstructure

Conference Paper *in* Lecture Notes in Computer Science · June 2009

DOI: 10.1007/978-3-642-12535-5_15 · Source: DBLP

2 authors, including:

Nikola Kosturski
Bulgarian Academy of Sciences
21 PUBLICATIONS **44** CITATIONS

SEE PROFILE

Numerical Homogenization of Bone Microstructure

Nikola Kosturski and Svetozar Margenov

Institute for Parallel Processing, Bulgarian Academy of Sciences

Abstract. The presented study is motivated by the development of methods, algorithms, and software tools for μFE (micro finite element) simulation of human bones. The voxel representation of the bone microstructure is obtained from a high resolution computer tomography (CT) image. The considered numerical homogenization problem concerns isotropic linear elasticity models at micro and macro levels.

Keywords: μFEM, nonconforming FEs, homogenization, bone microstructure.

1 Introduction

The reference volume element (RVE) of the studied trabecular bone tissue has a strongly heterogeneous microstructure composed of solid and fluid phases (see Fig. 1). In a number of earlier articles dealing with μFE simulation of bone structures (see, e.g., [8,10]), the contribution of the fluid phase is neglected. This simplification is the starting point for our study and for the related comparative analysis. In this study the fluid phase located in the pores of the solid skeleton is considered as almost incompressible linear elastic material. This means that the bulk modulus K_f is fixed and the related Poisson ration ν_f is approaching the incompressibility limit of 0.5. The elasticity modulus E_s and the Poisson ratio ν_s of the solid phase as well as the bulk modulus of the fluid phase K_f are taken from [4].

Let $\Omega \subset \mathbb{R}^3$ be a bounded domain with boundary $\Gamma = \Gamma_D \cup \Gamma_N = \partial\Omega$ and $\mathbf{u} = (u_1, u_2, u_3)$ be the *displacements* in Ω. The components of the *small strain tensor* are

$$\varepsilon_{ij} = \frac{1}{2}\left(\frac{\partial u_i}{\partial x_j} + \frac{\partial u_j}{\partial x_i}\right), \quad 1 \le i, j \le 3$$

and the components of the *Cauchy stress tensor* are

$$\sigma_{ij} = \lambda\left(\sum_{k=1}^{3} \varepsilon_{kk}\right)\delta_{ij} + 2\mu\varepsilon_{ij}, \quad 1 \le i, j \le 3.$$

Here λ and μ are the Lamé coefficients, which can be expressed by the elasticity modulus E and the Poisson ratio $\nu \in (0, 0.5)$ as follows

$$\lambda = \frac{E\nu}{(1+\nu)(1-2\nu)}, \quad \mu = \frac{E}{2+2\nu}.$$

I. Lirkov, S. Margenov, and J. Waśniewski (Eds.): LSSC 2009, LNCS 5910, pp. 140–147, 2010.

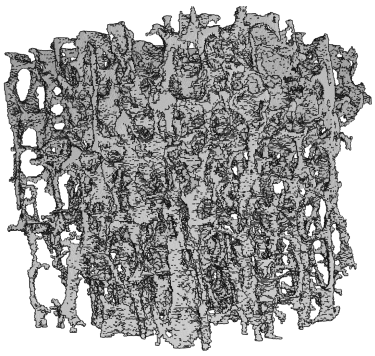

Fig. 1. Microstructure of a trabecular bone specimen

Now, we can introduce the Lamé's *system of linear elasticity* (see, e.g., [2])

$$\sum_{j=1}^{3} \frac{\partial \sigma_{ij}}{\partial x_j} + f_i = 0, \quad i = 1, 2, 3 \tag{1}$$

equipped with the boundary conditions

$$\begin{aligned} u_i(\mathbf{x}) &= g_i(\mathbf{x}), \quad \mathbf{x} \in \Gamma_D \subset \partial\Omega, \\ \sum_{j=1}^{3} \sigma_{ij}(\mathbf{x}) n_j(\mathbf{x}) &= h_i(\mathbf{x}), \quad \mathbf{x} \in \Gamma_N \subset \partial\Omega, \end{aligned}$$

where $n_j(\mathbf{x})$ are the components of the normal vector of the boundary for $\mathbf{x} \in \Gamma_N$.

The remainder of the paper is organized as follows. The applied locking-free nonconforming FEM discretization is presented in the next section. Section 3 contains a description of the applied numerical homogenization scheme. Selected numerical results are given in Section 4. The first test problem illustrates the locking-free approximation when the Poisson ratio tends to the incompressibility limit. Then, a set of numerical homogenization tests for real-life bone microstructures are presented and analyzed. Some concluding remarks are given at the end.

2 Locking-Free Nonconforming FEM Discretization

Let

$$\begin{aligned} (H_0^1(\Omega))^3 &= \left\{ \mathbf{u} \in (H^1(\Omega))^3 : \mathbf{u} = 0 \text{ on } \Gamma_D \right\}, \\ (H_g^1(\Omega))^3 &= \left\{ \mathbf{u} \in (H^1(\Omega))^3 : \mathbf{u} = \mathbf{g} \text{ on } \Gamma_D \right\}. \end{aligned}$$

The *weak formulation* of (1) can be written in the form (see, e.g., [3]): for a given $\mathbf{f} \in (L^2(\Omega))^3$ find $\mathbf{u} \in (H_g^1(\Omega))^3$ such that for each $\mathbf{v} \in (H_0^1(\Omega))^3$

$$a(\mathbf{u}, \mathbf{v}) = -\int_{\Omega} (\mathbf{f}, \mathbf{v}) dx + \int_{\Gamma_N} (\mathbf{h}, \mathbf{v}) dx.$$

In the case of pure displacement boundary conditions, the bilinear form $a(\cdot,\cdot)$ can be written as

$$a(\mathbf{u},\mathbf{v}) = \int_\Omega (Cd(\mathbf{u}), d(\mathbf{v})) = \int_\Omega (C^* d(\mathbf{u}), d(\mathbf{v})) = a^*(\mathbf{u},\mathbf{v}), \tag{2}$$

where

$$d(\mathbf{u}) = \left(\frac{\partial u_1}{\partial x_1}, \frac{\partial u_1}{\partial x_2}, \frac{\partial u_1}{\partial x_3}, \frac{\partial u_2}{\partial x_1}, \frac{\partial u_2}{\partial x_2}, \frac{\partial u_2}{\partial x_3}, \frac{\partial u_3}{\partial x_1}, \frac{\partial u_3}{\partial x_2}, \frac{\partial u_3}{\partial x_3}\right)^T$$

and the matrices C and C^* are

$$C = \begin{bmatrix}
\lambda+2\mu & 0 & 0 & 0 & \lambda & 0 & 0 & 0 & \lambda \\
0 & \mu & 0 & \mu & 0 & 0 & 0 & 0 & 0 \\
0 & 0 & \mu & 0 & 0 & 0 & \mu & 0 & 0 \\
0 & \mu & 0 & \mu & 0 & 0 & 0 & 0 & 0 \\
\lambda & 0 & 0 & 0 & \lambda+2\mu & 0 & 0 & 0 & \lambda \\
0 & 0 & 0 & 0 & 0 & \mu & 0 & \mu & 0 \\
0 & 0 & \mu & 0 & 0 & 0 & \mu & 0 & 0 \\
0 & 0 & 0 & 0 & 0 & \mu & 0 & \mu & 0 \\
\lambda & 0 & 0 & 0 & \lambda & 0 & 0 & 0 & \lambda+2\mu
\end{bmatrix},$$

$$C^* = \begin{bmatrix}
\lambda+2\mu & 0 & 0 & 0 & \lambda+\mu & 0 & 0 & 0 & \lambda+\mu \\
0 & \mu & 0 & 0 & 0 & 0 & 0 & 0 & 0 \\
0 & 0 & \mu & 0 & 0 & 0 & 0 & 0 & 0 \\
0 & 0 & 0 & \mu & 0 & 0 & 0 & 0 & 0 \\
\lambda+\mu & 0 & 0 & 0 & \lambda+2\mu & 0 & 0 & 0 & \lambda+\mu \\
0 & 0 & 0 & 0 & 0 & \mu & 0 & 0 & 0 \\
0 & 0 & 0 & 0 & 0 & 0 & \mu & 0 & 0 \\
0 & 0 & 0 & 0 & 0 & 0 & 0 & \mu & 0 \\
\lambda+\mu & 0 & 0 & 0 & \lambda+\mu & 0 & 0 & 0 & \lambda+2\mu
\end{bmatrix}.$$

Let us note, that the modified bilinear form $a^*(\cdot,\cdot)$ is equivalent to $a(\cdot,\cdot)$ if

$$\int_\Omega \frac{\partial u_i}{\partial x_j}\frac{\partial u_j}{\partial x_i}dx = \int_\Omega \frac{\partial u_i}{\partial x_i}\frac{\partial u_j}{\partial x_j}dx \tag{3}$$

is fulfilled. It is also important, that the rotations are excluded from the kernel of the modified (corresponding to $a^*(\cdot,\cdot)$) Neumann boundary conditions operator. As a result, the nonconforming Crouzeix-Raviart (C.–R.) FEs are applicable to the modified variational problem, providing a locking-free discretization. Locking-free error estimates of the 2D pure displacement problem discretized by C.–R. FEs are presented, e.g., in [3]. A similar analysis is applicable to the 3D case as well.

It is easy to check that the equality (3) holds true also for the RVE with Dirichlet boundary conditions with respect to the normal displacements only. As we will see in the next section, this is exactly the case in the studied numerical homogenization scheme.

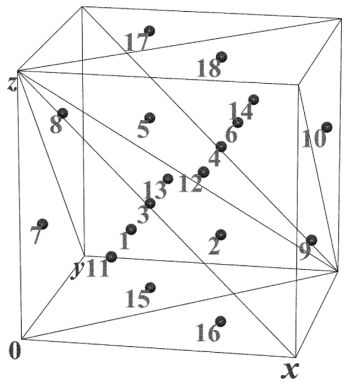

Fig. 2. Splitting a voxel into six tetrahedra

In order to apply C.–R. FE discretization of RVE, we split each voxel (macroelement) into six tetrahedra, see Fig. 2. For a RVE divided into $n \times n \times n$ voxels, the number of unknowns in the resulting linear system is $18n^2(2n+1)$. A block factorization (static condensation) is applied first on the macroelement level, eliminating the unknowns associated with the inner nodes. This step reduces the total number of unknowns to $18n^2(n+1)$.

3 Numerical Homogenization

We study the implementation of a standard numerical homogenization scheme of Dirichlet boundary conditions type [6]. The RVE boundary value problem has zero normal displacements on five of the faces of the cube and a (small) nonzero constant normal displacement on the sixth face (see Fig. 3). The right hand side is also supposed to be zero. Nonconforming C.–R. finite elements (based on the modified bilinear form $a^*(\cdot,\cdot)$ from (2)) are used to get a locking-free discretization.

By symmetry arguments, it simply follows that the homogenized stress and the strain tensors have zero shear components, and therefore the following relation between the homogenized normal stress and strain components holds

$$\begin{bmatrix} \hat{\sigma}_x \\ \hat{\sigma}_y \\ \hat{\sigma}_z \end{bmatrix} = \frac{E(1-\nu)}{(1+\nu)(1-2\nu)} \begin{bmatrix} 1 & \frac{\nu}{1-\nu} & \frac{\nu}{1-\nu} \\ \frac{\nu}{1-\nu} & 1 & \frac{\nu}{1-\nu} \\ \frac{\nu}{1-\nu} & \frac{\nu}{1-\nu} & 1 \end{bmatrix} \begin{bmatrix} \hat{\varepsilon}_x \\ \hat{\varepsilon}_y \\ \hat{\varepsilon}_z \end{bmatrix}.$$

Let us consider now the case, where the nonzero constant normal displacement (in z direction) is applied on the top face of the RVE cube. Then $\hat{\varepsilon}_x = \hat{\varepsilon}_y = 0$ and therefore

$$\hat{\sigma}_x = \hat{\sigma}_y = \frac{E\nu}{(1+\nu)(1-2\nu)}\hat{\varepsilon}_z, \quad \text{and} \quad \hat{\sigma}_z = \frac{E(1-\nu)}{(1+\nu)(1-2\nu)}\hat{\varepsilon}_z.$$

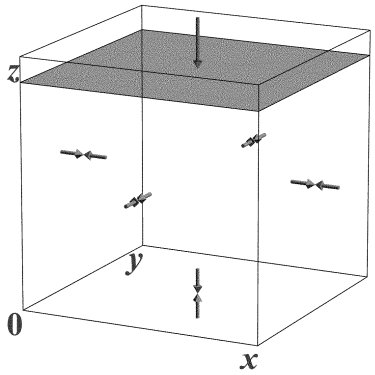

Fig. 3. Boundary conditions of the RVE problem

From these relations we can directly calculate the homogenized elasticity coefficients as follows

$$\nu = \frac{1}{1+p}, \quad E = \frac{(1+\nu)(1-2\nu)}{1-\nu} r,$$

where

$$p = \frac{\hat{\sigma}_z}{\hat{\sigma}_x} = \frac{\hat{\sigma}_z}{\hat{\sigma}_y}, \quad r = \frac{\hat{\sigma}_z}{\hat{\varepsilon}_z}.$$

In theory $\hat{\sigma}_x = \hat{\sigma}_y$. In the case of numerical homogenization, the average values of the stresses σ_x and σ_y over all tetrahedral finite elements are used. In the case of numerical homogenization of strongly heterogeneous materials (like bone tissues), the average stresses $\hat{\sigma}_x$ and $\hat{\sigma}_y$ are not equal. This is why we set

$$\hat{\sigma}_x = \hat{\sigma}_y = \frac{1}{2}\left(\frac{1}{N_{el}}\sum_{i=1}^{N_{el}} \sigma_x^i + \frac{1}{N_{el}}\sum_{i=1}^{N_{el}} \sigma_y^i\right)$$

when computing the homogenized elasticity modulus and Poisson ratio.

Similar relations hold when the nonzero displacements are alternatively applied in the x and y directions. To determine the elasticity coefficients more precisely, we apply the above numerical scheme in all three cases, and finally average the computed elasticity modulus and Poisson ratio.

4 Numerical Experiments

A set of numerical tests illustrating the accuracy of the locking-free FEM approximation in the almost incompressible case are presented first. The second part of the section contains results of numerical homogenization of three real-life

Table 1. Relative error on a fixed $32 \times 32 \times 32$ mesh for $\nu \to 0.5$

ν	$\|\mathbf{r}\|_\infty$	$\|\mathbf{f}\|_\infty$	$\|\mathbf{r}\|_\infty / \|\mathbf{f}\|_\infty$
0.4	0.033733	214407	1.57331×10^{-7}
0.49	0.052206	1381450	3.77904×10^{-8}
0.499	0.551943	13125600	4.20509×10^{-8}
0.4999	5.551980	1.31×10^{8}	4.24652×10^{-8}
0.49999	55.552900	1.31×10^{9}	4.25009×10^{-8}

bone microstructure RVEs. The (additional) response of the fluid phase within the studied linear elasticity model is analyzed.

The studied methods and algorithms are addressed to the case of μFEM numerical homogenization which leads in general to large-scale linear systems. The developed solver is based on the Preconditioned Conjugate Gradient (PCG) [1] method, where BoomerAMG[1] is used as a preconditioner (see also [7] for an alternative locking-free AMLI solver in 2D). In the presented numerical tests, the relative stopping criterion for the PCG method is $\mathbf{r}_k^T C^{-1} \mathbf{r}_k \leq 10^{-12} \mathbf{r}_0^T C^{-1} \mathbf{r}_0$. The numerical tests are run on an IBM Blue Gene/P supercomputer.

4.1 Model Problem

A homogeneous material with fixed elasticity modulus $E = 0.06\,\mathrm{GPa}$ is considered. The computational domain Ω is the unit cube $[0,1]^3$. A pure displacement problem is considered with Dirichlet boundary conditions on $\Gamma_D = \partial\Omega$ corresponding to the given exact solution

$$\begin{aligned} u_1(x,y,z) &= x^3 + \sin(y+z), \\ u_2(x,y,z) &= y^3 + z^2 - \sin(x-z), \\ u_3(x,y,z) &= x^2 + z^3 + \sin(x-y). \end{aligned}$$

The right hand side $\mathbf{f}$ is obtained by substituting the exact solution and the corresponding material coefficients in Lamé's system (1). The relative errors presented in Table 1 well illustrate the robustness (locking-free approximation) of the C.–R. nonconforming FEM approximation of almost incompressible elasticity problems.

4.2 Homogenization of Bone Microstructures

Three test cases of different RVE are considered. The related voxel representations ($16 \times 16 \times 16$, $32 \times 32 \times 32$ and $64 \times 64 \times 64$) of the bone microstructure are extracted from a high resolution computer tomography (CT) image [9]. The used mechanical properties of bones are from [4]. The elasticity modulus of solid phase is $E_s = 14.7\,\mathrm{GPa}$ and the related Poisson ratio is $\nu_s = 0.325$. The fluid phase is considered as almost incompressible where the bulk modulus $K_f = 2.3\,\mathrm{GPa}$ is

[1] BoomerAMG is a parallel algebraic multigrid implementation from the package Hypre, developed in LLNL, Livermore [5].

Table 2. Solid skeleton: $E_s = 14.7$ GPa, $\nu_s = 0.325$

	$16 \times 16 \times 16$	$32 \times 32 \times 32$	$64 \times 64 \times 64$
Solid phase	47 %	26 %	19 %
E_{hom}	3.21 GPa	1.10 GPa	0.58 GPa
ν_{hom}	0.118	0.141	0.158

Table 3. Solid skeleton with incompressible fluid filling: RVE of $16 \times 16 \times 16$ voxels

Solid phase		Fluid phase		Homogenized	
E_s	ν_s	E_f	ν_f	E_{hom}	ν_{hom}
14.7 GPa	0.325	1.38×10^8 Pa	0.49	5.05 GPa	0.299
14.7 GPa	0.325	1.38×10^7 Pa	0.499	4.82 GPa	0.307
14.7 GPa	0.325	1.38×10^6 Pa	0.4999	4.79 GPa	0.309
14.7 GPa	0.325	1.38×10^5 Pa	0.49999	4.79 GPa	0.309
14.7 GPa	0.325	1.38×10^4 Pa	0.499999	4.79 GPa	0.309

Table 4. Solid skeleton with incompressible fluid filling: RVE of $32 \times 32 \times 32$ voxels

Solid phase		Fluid phase		Homogenized	
E_s	ν_s	E_f	ν_f	E_{hom}	ν_{hom}
14.7 GPa	0.325	1.38×10^8 Pa	0.49	2.24 GPa	0.376
14.7 GPa	0.325	1.38×10^7 Pa	0.499	1.96 GPa	0.391
14.7 GPa	0.325	1.38×10^6 Pa	0.4999	1.88 GPa	0.396
14.7 GPa	0.325	1.38×10^5 Pa	0.49999	1.86 GPa	0.396
14.7 GPa	0.325	1.38×10^4 Pa	0.499999	1.86 GPa	0.396

Table 5. Solid skeleton with incompressible fluid filling: RVE of $64 \times 64 \times 64$ voxels

Solid phase		Fluid phase		Homogenized	
E_s	ν_s	E_f	ν_f	E_{hom}	ν_{hom}
14.7 GPa	0.325	1.38×10^8 Pa	0.49	1.54 GPa	0.408
14.7 GPa	0.325	1.38×10^7 Pa	0.499	1.19 GPa	0.428
14.7 GPa	0.325	1.38×10^6 Pa	0.4999	1.07 GPa	0.435
14.7 GPa	0.325	1.38×10^5 Pa	0.49999	1.05 GPa	0.436
14.7 GPa	0.325	1.38×10^4 Pa	0.499999	1.05 GPa	0.436

known. In the presented tests, the Poisson ratio is ν_f varied between 0.49 and $0.5 - 10^{-6}$, and respectively $E_f = 3K_f(1 - 2\nu_f)$. Tables 3, 4, and 5 contain the homogenized material coefficients of three bone specimens with different mesh sizes. The case when the fluid phase is neglected is presented in Table 2, including the percentage of the solid phase of the considered three RVEs. This is the starting point of our comparative analysis.

The last three tables clearly demonstrate the significant contribution of the fluid phase to the homogenized parameters (E_{hom}, ν_{hom}). The numerical stability with respect to $\nu_f \to 0.5$ is also well expressed. High accuracy of the homogenization procedure is achieved for $\nu_f \in \{0, 4999,\ 0.499999\}$.

The following next steps in the numerical homogenization of bone microstructures are planned: a) anisotropic macro model; b) poroelasticity micro model. The goal is to improve further (quantitatively and qualitatively) our understanding of the underlying phenomena.

Acknowledgments

This work is partly supported by the Bulgarian NSF Grants DO02-115/08 and DO02-147/08. We kindly acknowledge also the support of the Bulgarian Supercomputing Center for the access to the supercomputer IBM Blue Gene/P.

References

1. Axelsson, O.: Iterative solution methods. Cambridge University Press, Cambridge (1994)
2. Axelsson, O., Gustafsson, I.: Iterative methods for the Navier equations of elasticity. Comp. Meth. Appl. Mech. Engin. 15, 241–258 (1978)
3. Brenner, S., Sung, L.: Nonconforming finite element methods for the equations of linear elasticity. Math. Comp. 57, 529–550 (1991)
4. Cowin, S.: Bone poroelasticity. J. Biomechanics 32, 217–238 (1999)
5. Lawrence Livermore National Laborary, Scalable Linear Solvers Project, `https://computation.llnl.gov/casc/linear_solvers/sls_hypre.html`
6. Kohut, R.: The determination of Young modulus E and Poisson number ν of geocomposite material using mathematical modelling, private communication (2008)
7. Kolev, T., Margenov, S.: Two-level preconditioning of pure displacement nonconforming FEM systems. Numer. Lin. Algeb. Appl. 6, 533–555 (1999)
8. Margenov, S., Vutov, Y.: Preconditioning of Voxel FEM Elliptic Systems. TASK, Quaterly 11(1-2), 117–128 (2007)
9. Vertebral Body Data Set ESA29-99-L3, `http://bone3d.zib.de/data/2005/ESA29-99-L3`
10. Wirth, A., Flaig, C., Mueller, T., Müller, R., Arbenz, P., van Lenthe, G.H.: Fast Smooth-surface micro-Finite Element Analysis of large-scale bone models. J. Biomechanics 41 (2008), doi:10.1016/S0021-9290(08)70100-3